Earthquakes and Structures, *Vol. 12, No. 5 (2017) 501-513*
DOI: https://doi.org/10.12989/eas.2017.12.5.501

Shake table test of Y-shaped eccentrically braced frames fabricated with high-strength steel

Ming Lian[1,2a] and Mingzhou Su[*1]

[1]*School of Civil Engineering, Xi'an University of Architecture and Technology, Xi'an 710055, P.R. China*
[2]*Post-doctoral Mobile Stations of Material Science and Engineering, Xi'an University of Architecture and Technology, Xi'an 710055, P.R. China*

(Received December 16, 2016, Revised April 19, 2017, Accepted April 20, 2017)

Abstract. To investigate the seismic performance of Y-shaped eccentrically braced frames fabricated with high-strength steel (Y-HSS-EBFs), a shake table test of a 1:2 scaled three-story Y-HSS-EBF specimen was performed. The input wave for the shake table test was generated by the ground motions of El Centro, Taft, and Lanzhou waves. The dynamic properties, acceleration, displacement, and strain responses were obtained from the test specimen and compared with previous test results. In addition, a finite element model of the test specimen was established using the SAP2000 software. Results from the numerical analysis were compared with the test specimen results. During the shake table test, the specimen exhibited sufficient overall structural stiffness and safety but suffered some localized damage. The lateral stiffness of the structure degenerated during the high seismic intensity earthquake. The maximum elastic and elastoplastic interstory drift of the test specimen for different peak ground accelerations were 1/872 and 1/71, respectively. During the high seismic intensity earthquake, the links of the test specimen entered the plastic stage to dissipate the earthquake energy, while other structural members remained in the elastic stage. The Y-HSS-EBF is a safe, dual system with reliable seismic performance. The numerical analysis results were in useful agreement with the test results. This finding indicated that the finite element model in SAP2000 provided a very accurate prediction of the Y-HSS-EBF structure's behavior during the seismic loadings.

Keywords: eccentrically braced frames (EBFs); high-strength steel (HSS); shake table test; dynamic properties; seismic performance; numerical simulation

1. Introduction

Eccentrically braced frames (EBFs) have evolved from moment-resisting frames (MRFs) and concentrically braced frames (CBFs). MRFs offer high ductility and energy dissipation capabilities but have low stiffness. Comparatively, CBFs have higher stiffness but lower energy dissipation capabilities. EBFs were developed by incorporating the best features offered by both MRFs and CBFs. Earthquake energy can be dissipated through the plastic deformation of EBF links.

Significant contributions to the understanding of the seismic performance of an EBF were made during the 1980s. The researchers have studied wildly on the seismic performance, design method and new structural types so far. Mansour *et al.* studied the cyclic performance of EBFs with different types of replaceable shear links (Mansour *et al.* 2011). The experimental results indicated that the links exhibited a very good ductile behavior, developing stable and repeatable yielding and the inelastic rotation capacity could be achieved with bolted replaceable links when bolt bearing deformations were allowed to occur. The effect of shear-moment interaction in the plastic design of EBFs was studied by Montuori *et al.* (Montuori *et al.* 2014, Montuori *et al.* 2014), where a procedure for determining the ultimate link shear force and link end moments was proposed for a given collapse mechanism. Shayanfar *et al.* tested new type of shear link which was steel and reinforced concrete composite vertical shear link, as seen in Fig. 1 (Shayanfar *et al.* 2012). In this shear link, the reinforced concrete was located at the area surrounded by the web and flanges of the steel section and the reinforced concrete in the link could be

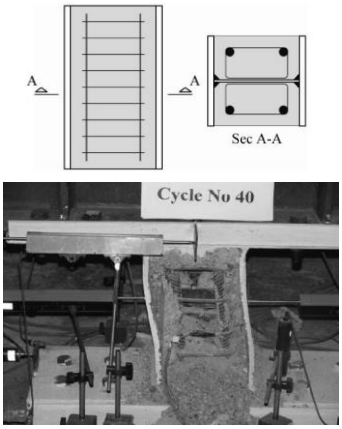

Fig. 1 Composite vertical shear link (Shayanfar *et al.*)

*Corresponding author, Professor
E-mail: sumingzhou@163.com
[a]Ph.D.
E-mail: lianming0821@163.com.

ISSN: 2092-7614 (Print), 2092-7622 (Online)

considered as the stiffeners. Results revealed that the concrete in the links could delay the web buckling and increase the shear strength and energy dissipation of the specimens significantly.

Over time, improvements in the mechanical properties and weldability of high-strength steel (HSS), along with the availability of improved welding consumables and processes, have made HSS an economical alternative to conventional steel in EBF constructions. Moreover, as HSS has a higher strength than conventional steel, HSS structural members can have smaller cross-sections than those of conventional steel members under the same design conditions. This reduces the weight of the structure and improves economy through reduced material costs. HSS has been widely used in bridge structures (Shim *et al.* 2011, Chen *et al.* 2012), and it has begun to appear in building structure designs (Tokgoz *et al.* 2012, Wang *et al.* 2014). Furthermore, Longo et al. used HSS in the MR-Frames, in which the beams used the normal steel and the columns used HSS (Longo *et al.* 2014). The results indicated that using HSS in this structure could reduce the structural weight and cost, showing the convenience of the structure designed by means of HSS.

EBFs fabricated with high-strength steel (HSS-EBFs) combine the advantages of HSS and EBFs. In HSS-EBFs, links and braces generally use conventional steel, while columns and beams are made of HSS. Braces using HSS may result in larger sections and increased material costs than those using conventional steel. As a point of reference, "conventional steel" is defined as steel with a specified nominal yield stress of up to 345 MPa. On the contrary, "HSS" is defined as steel with a specified nominal yield stress above 345 MPa. HSS-EBFs are designed such that the columns and beams remain in the elastic stage or experience only a slight plastification, while the links fully enter the plastic stage during rare earthquake motions (2% probability of exceedance in a 50-year period).

Many theoretical and experimental studies have been performed to determine the mechanical behavior and seismic performance of EBFs (Berman and Bruneau 2007, Dubina 2008, Bosco and Rossi 2009, Dusicka 2010, Lin *et al.* 2011), but few have included shake table tests of the structural system. The objective of this study was to use a shake table test to experimentally investigate the overall dynamic behavior of a three-story Y-shaped HSS-EBF (Y-HSS-EBF) specimen. A finite element model (FEM) of the test specimen was also constructed using the SAP2000 software. Moreover, a comparison between the experimental and numerical results was performed.

2. Design of specimen and test scheme

2.1 Test specimen

The prototype structure was designed according to the GB50010-2010 and JGJ99-98 codes. The site for the prototype structure was characterized by peak ground acceleration (PGA) of 0.2 g with a 10% exceedance probability in 50 years and moderately firm ground conditions. A three-story, one-bay Y-HSS-EBF was considered the prototype structure for this study. Fig. 2 depicts the prototype structure.

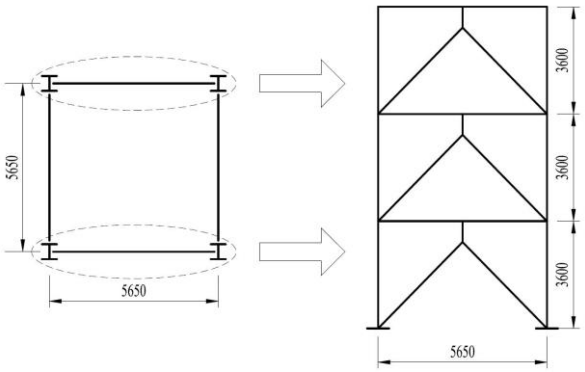

Fig. 2 Dimensions of prototype structure

The shake table's 4 m×4 m size and maximum vertical load carrying capacity of 300 kN limited the size and strength capacity (i.e., the maximum base shear and overturning moment) of the test specimen obtained from the prototype structure. To fully utilize the shake table, the span of the test specimen was designed to be 2.825 m. Thus, the scaling factor for length was calculated as

$$S_l = \frac{2.825}{5.650} = 0.5 \tag{1}$$

The material composition of the test specimen was identical to that of the prototype structure, suggesting a scaling factor for the elastic modulus equal to one (S_E=1). To keep the total weight of the test specimen less than the maximum vertical load carrying capacity of the shake table without reducing the horizontal earthquake forces, the similarity ratio of acceleration was taken as S_a=1.2 (the factor did not control the gravity acceleration). Similar relationships were derived for other parameters by using similar theory (Li 2004), as summarized in Table 1.

Table 1 Similarity relationships and ratios of the test specimen

Physical quantities	Dimensions	Similarity relation	Ratio of similarity
Strain	—	$S_\varepsilon = 1$	1
Elastic modulus	FL^{-2}	$S_E = 1$	1
Stress	FL^{-2}	$S_\sigma = S_E\, S_\varepsilon$	1
Length	L	$S_l = 0.5$	0.5
Force	F	$S_F = S_\sigma\, S_l^2 = S_E\, S_\varepsilon S_l^2$	0.25
Mass	FT^2L^{-1}	$S_m = S_F/S_a = (S_E\, S_\varepsilon S_l^2)/S_a$	0.2083
Density	FT^2L^{-4}	$S_\rho = S_m/S_l^3 = (S_E\, S_\varepsilon)/(S_a S_l)$	1.6667
Time/nature period	T	$S_t = S_T = (S_l/S_a)^{-1/2}$	0.6455
Frequency	T^{-1}	$S_f = 1/S_T = (S_l/S_a)^{-1/2}$	1.5492
Displacement	L	$S_x = S_l$	0.5
Acceleration	LT^{-2}	$S_a = 1.2$	1.2

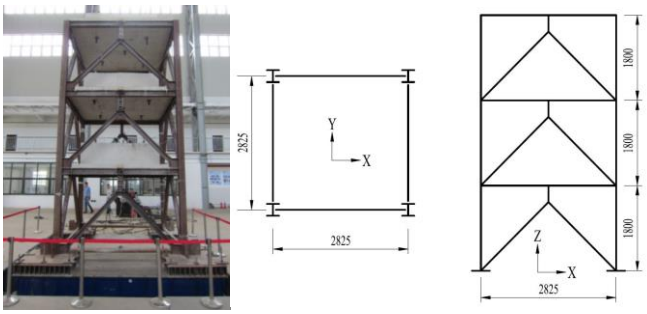

(a) Test specimen (b) Elevation and plan view of test specimen

Fig. 3 Dimensions of test specimen (dimensions in mm)

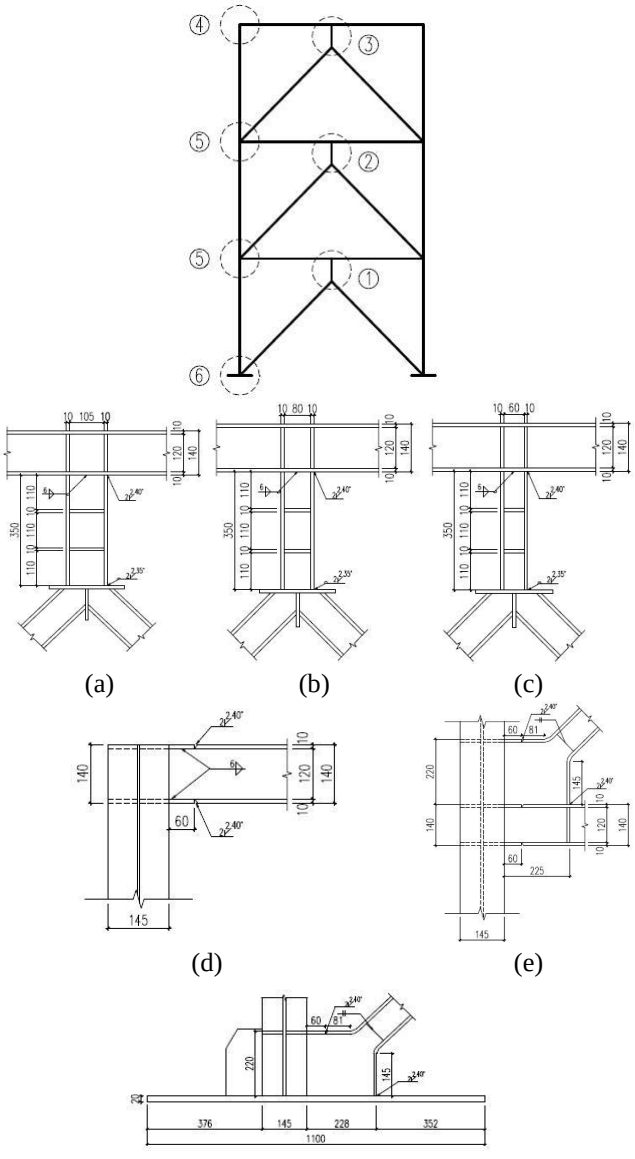

Fig. 4 Details of joints

The test specimen was constructed as a three-story Y-HSS-EBF with shear links and a single bay in both the x- and y-directions, as shown in Fig. 3. The story height, x-direction span, and y-direction span were 1.8 m, 2.825 m, and 2.825 m, respectively. The thickness of the reinforced concrete floor was 80 mm. The links used Q235 steel (steel with specified nominal yield strength of 235 MPa), while the braces, columns, and beams used Q460 steel (steel with specified nominal yield strength of 460 MPa). The mechanical properties of the steel used in the test specimen are summarized in Table 2. The length of the shear links was 350 mm. Welded joints were used to connect the links to the beams and other elements of the test specimen. Table 3 lists the structural member sections. The details of the joint characteristics are shown in Fig. 4.

Table 2 Mechanical properties of steel

Steel	Thickness	Yield stress	Ultimate strength	Elastic modulus	Elongation ratio
	t (mm)	f_y (MPa)	f_u (MPa)	E (×10^5 MPa)	(%)
Q235	3	283.1	397.1	2.14	31.57
Q235	4	271.9	402.1	2.17	31.83
Q235	8	276.7	421.1	2.18	32.18
Q345	6	414.7	542.03	2.11	28.29
Q345	10	363.8	545.8	2.01	28.74
Q460	8	473.5	635.1	2.12	25.36
Q460	10	516.0	692.0	2.06	23.51

Table 3 Member sections of the specimen

Structural members	Story number		
	1	2	3
Links	H125×70×4×8	H100×70×4×8	H80×70×3×8
Beams	H140×100×8×10	H140×100×8×10	H140×100×8×10
Columns	H145×145×8×10	H145×145×8×10	H145×145×8×10
Braces	H100×100×6×10	H100×100×6×10	H100×100×6×10

Note: "H" refers to the welded H-shaped section, the following numbers are the section depth (h), flange width (b_f), web thickness (t_w), and flange thickness (t_f), with units of mm.

Dead loads of 5 kN/m^2 for each floor and 5.625 kN/m^2 for the roof, live loads of 2 kN/m^2 for each floor, and wall loads of 4.38 kN/m^2 were considered. Representative values of gravity equal to 1D+0.5L were applied, where D and L are dead and live loads, respectively. Considering the dead and live loads, the total mass for the test specimen was 23.8 t.

2.2 Instrument arrangement

To characterize the dynamic behavior of Y-HSS-EBF structures, the objectives of this experiment were to obtain the dynamic strain response, acceleration response, and displacement response for the test specimen floors. As shown in Fig. 5, 16 accelerometers (A1-A16) were used; four were placed on each of the three floors and on the base plate in the x-direction. Thirteen strain gauges were placed on the links of each story (C1-C5, C13-C17, and C22-C24) in the x-direction and on other structural members (C6-C12, C18-C21, and C25-C26). Eight displacement sensors (D1-D8) were used; two were placed on each of the three floors and on the base plate.

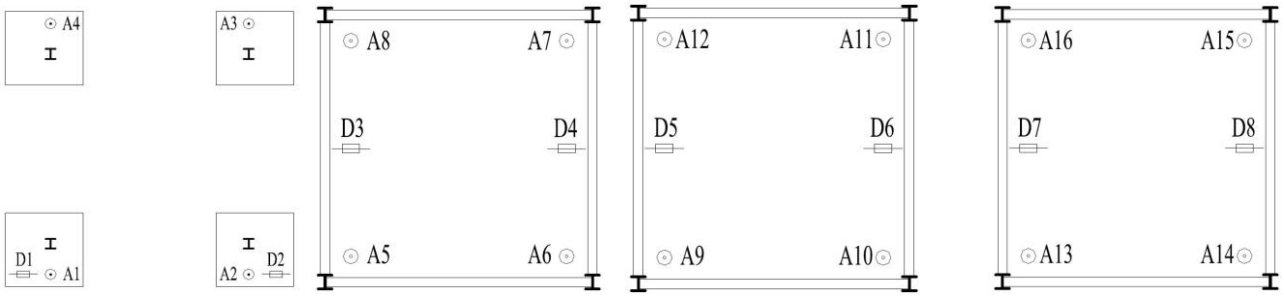

layout of accelerometers on top of base plate | layout of accelerometers on first floor | layout of accelerometers on second floor | layout of accelerometers on roof

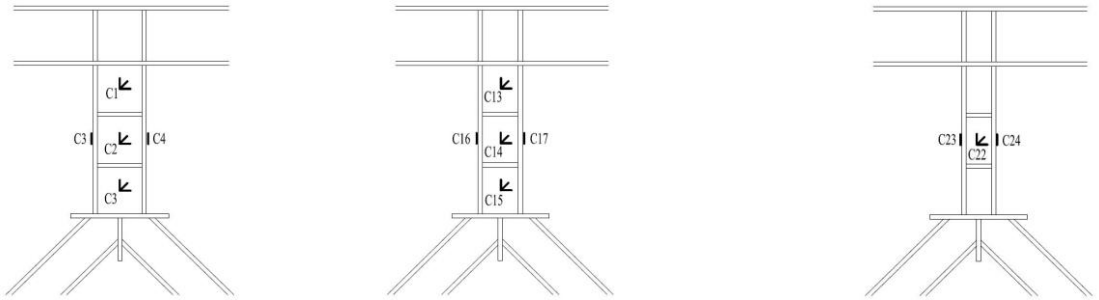

layout of strain gauges on first story link | layout of strain gauges on second story link | layout of strain gauges on third story link

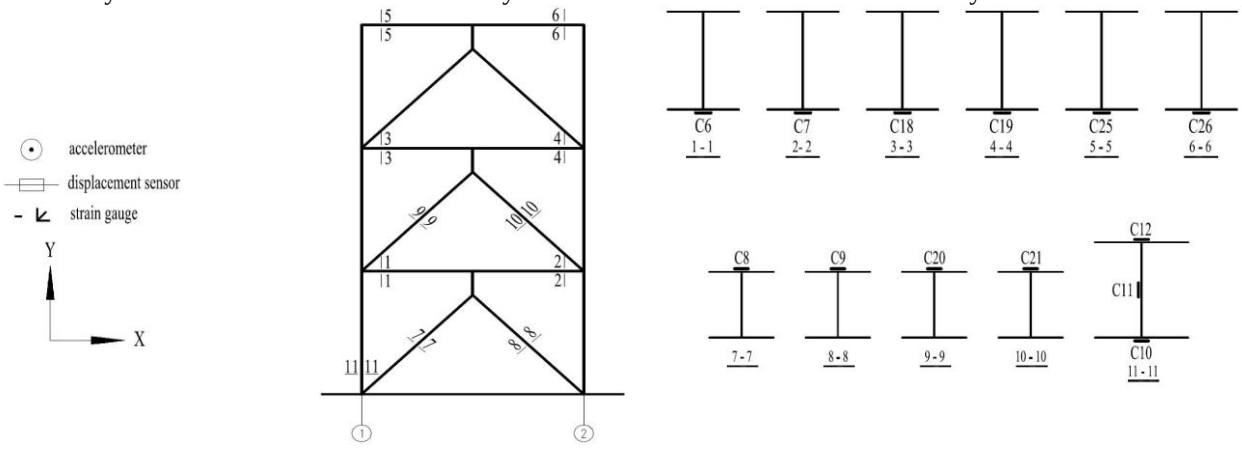

layout of strain gauges on braces, beams, and columns

Fig. 5 Layout of sensors

2.3 Seismic loadings

To investigate the effects of different ground motions on the seismic performance of the three-story Y-HSS-EBF specimen, three different ground motions were selected as input excitations for the shake table test, according to requirements in GB50011-2010: the El Centro wave (1940), the Taft wave (1952), and the Lanzhou artificial wave. Fig. 6 shows the time histories for the three ground motions after compression by the time similarity ratio (refer to Table 1). Fig. 7 shows the acceleration response spectra of the accelerogram ensemble, along with the design acceleration spectrum. Moreover, the effects of seismic excitation intensity on the seismic performance of the model were considered using increased seismic loadings. For each seismic excitation intensity, the acceleration of the three ground motions were scaled to the corresponding PGA of the seismic intensity (refer to Table 4). A white noise frequency test was applied to measure the dynamic behavior of the test specimen before each PGA level. Loading was in the *x*-direction along the Y-shaped braced frame (refer to Fig. 2). Table 4 details all loading cases for the shake table test, where WN is the white noise wave, and PGA is the peak value of the input accelerogram. Furthermore, three structural performance levels, i.e., immediate occupancy, life safety, and collapse prevention limit states, were considered for the system assessment carried out in the present study. These limit states comply with seismic suggestions by FEMA 356. The relationships between seismic performance and the loading cases (refer to Table 4) are summarized in Table 5. Additionally, the prototype structure of the specimen was designed for a PGA of 0.2 g with a 10% exceedance probability in 50 years, while the similarity ratio of acceleration was defined as S_a = 1.2 for

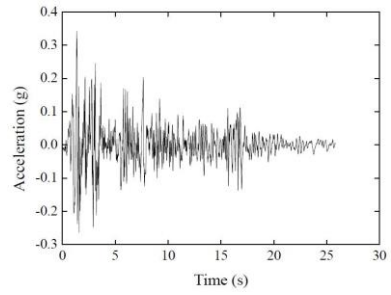

(a) El Centro

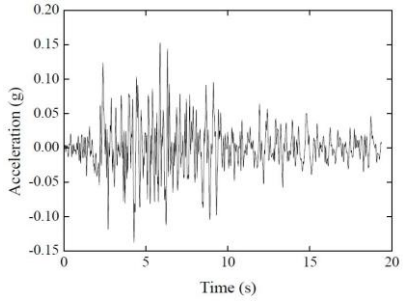

(b) Taft

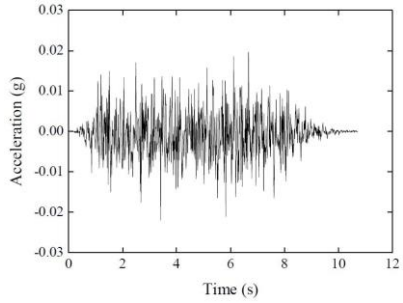

(c) Lanzhou

Fig. 6 Acceleration time histories of input ground motions

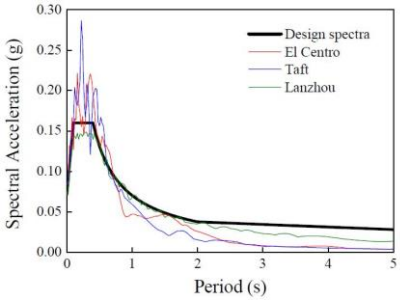

Fig. 7 Spectra comparison of earthquakes with 50% probability of exceedance in 50 years

the shake table test. Thus, the corresponding PGA for the "life safety" level was 0.24 g, as shown in Table 5.

3. Test results and discussion

3.1 Test phenomena

During each level of seismic loading, the test specimen's cumulative structural damage and plastic deformation increased, while its stiffness decreased. When the PGA

Table 4 List of test cases

Case	Earthquake	PGA (g)
WN1	WN	0.05
1	El Centro	
2	Taft	0.042
3	Lanzhou	
WN2	WN	0.05
4	El Centro	
5	Taft	0.084
6	Lanzhou	
WN3	WN	0.05
7	El Centro	
8	Taft	0.12
9	Lanzhou	
WN4	WN	0.05
10	El Centro	
11	Taft	0.168
12	Lanzhou	
WN5	WN	0.05
13	El Centro	
14	Taft	0.24
15	Lanzhou	
WN6	WN	0.05
16	El Centro	
17	Taft	0.264
18	Lanzhou	
WN7	WN	0.05
19	El Centro	
20	Taft	0.48
21	Lanzhou	
WN8	WN	0.05
22	El Centro	
23	Taft	0.744
24	Lanzhou	
WN9	WN	0.05
25	El Centro	
26	Taft	1
27	Lanzhou	
WN10	WN	0.05

Table 5 Limit states (FEMA 356)

Performance level	Qualitative description	Recommended drifts (EBF) (%)	Corresponding PGAs in Table 4
SP-1	Immediate occupancy	0.5	0.084 g
SP-2	Life safety	1.5	0.24 g
SP-3	Collapse prevention	2.0	0.48 g

(a) Rust dropped off from joint

(b) Rust dropped off from link web

(c) Residual deformation of first-story link

(d) Residual deformation of third-story link

(e) Weld fractured at link-to-beam joint

(f) Weld fractured at link-to-braces joint

Fig. 8 Test phenomena

Table 6 Test phenomena

Case	PGA (g)	Description of test phenomena
Case 1-3	0.042	No obvious phenomenon in the elastic region
Case 4-6	0.084	No obvious phenomenon in the elastic region
Case 7-9	0.12	No obvious phenomenon in the elastic region
Case 10-12	0.168	No obvious phenomenon in the elastic region
Case 13-15	0.24	No obvious phenomenon in the elastic region
Case 16-18	0.264	Rust dropped off from the weld of link-to-brace joint, as shown in Fig. 8(a); Rust dropped off from the weld in links as shown in Fig. 8(b)
Case 19-21	0.48	Residual deformation occurred in the links in the first and third stories, as shown in Fig. 8(c) and Fig. 8(d)
Case 22-24	0.744	Through weld cracks appeared at link-to-beam joint in the third story, as shown in Fig. 8(e)
Case 25-27	1.0	Disconnected weld fracture appeared at link-to-braces joint in the third story, as shown in Fig. 8(f)

reached 0.48 g, plastic deformation of the links occurred, and residual link deformation appeared in the first and third stories. When the PGA reached 0.744 g, through cracks appeared at the welds located between link and beam in the third story. When the PGA reached 1.0 g, disconnected weld fracture appeared at link-to-braces joint in the third story. No plastic deformation was observed in the braces, beams, or columns. Table 6 lists the test phenomena observed at different PGA levels.

3.2 Dynamic characteristics

Table 7 Natural frequencies and damping ratios of the test specimen

Case	Natural frequency (Hz)	Damping ratio (%)
WN1	5.48	2.99
WN 2	5.48	3.04
WN 3	5.48	3.09
WN 4	5.46	3.17
WN 5	5.45	3.23
WN 6	5.19	3.49
WN 7	4.76	3.81
WN 8	4.32	4.36
WN 9	4.18	4.59
WN 10	3.42	6.03

White noise sweeps were used to obtain the first natural frequencies of the test specimen in the *x*-direction. As shown in Table 7, the initial frequency and damping ratio reached up to 5.48 Hz and 2.99%, respectively. The natural frequency decreased by 37.6% in the x-direction after the test.

The frequency, *f*, was estimated using the following equation

$$f = \frac{1}{2\pi}\sqrt{\frac{k}{m}} \tag{2}$$

where k is the lateral stiffness and m is the mass of the structure. Eq. (2) indicates that the stiffness k is proportional to the quadratic frequency f^2, when the mass m is constant. Thus, a change in natural frequency reflects a change in the stiffness of the test specimen.

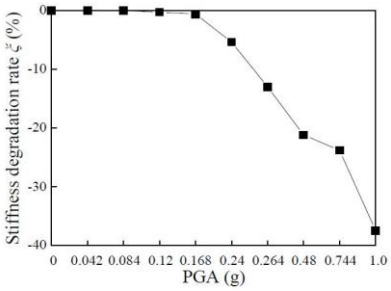

Fig. 9 Structural stiffness degradation

The stiffness degradation rate of the specimen ξ was determined by the following equation

$$\xi = \frac{k_0 - k}{k_0} = \frac{f_0^2 - f^2}{f_0^2} \tag{3}$$

where k and f are the lateral stiffness and the natural frequency of the specimen after the dynamic load, respectively; k_0 and f_0 are the initial lateral stiffness and the initial natural frequency, respectively. Fig. 9 shows the stiffness degradation of the specimen given by Eq. (3). The stiffness clearly degraded as PGAs increased from 0.48 g to 0.744 g and 1.0 g. Specimen stiffness decreased by 37.6% in the *x*-direction. The specimen was observed to have serious cumulative damage and plastic deformation after the test.

3.3 Acceleration response

To study the acceleration response of the specimen, the peak acceleration value of each story was divided by that of the structure base. The acceleration amplification factor λ was defined as follows

$$\lambda = \frac{a_2}{a_1} \tag{4}$$

where a_1 represents the output acceleration of the base of the specimen, and a_2 represents the output acceleration of each story. Acceleration amplification factors for each measured point on the specimen were calculated. Fig. 10 shows the dynamic enlargement curves for each story under seismic loading.

The acceleration response increased along the height of the specimen. When PGAs increase, the dynamic response curves followed similar trends. With incremental increases in seismic intensity, the acceleration amplification factor curves for each story decreased, indicating an accumulation of plastic damage and a degradation of lateral stiffness in the specimen.

3.4 Displacement response

Displacement response measurements at each story and the base were obtained using displacement sensors. Fig. 11 shows the maximum relative story displacement in the *x*-direction. When acceleration was less than 0.48 g, the displacements of each story were nearly proportional, suggesting minimal damage to the specimen. However, the

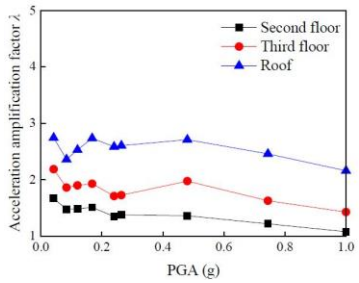

(a) El Centro wave

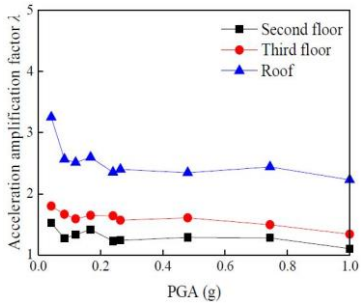

(b) Taft wave

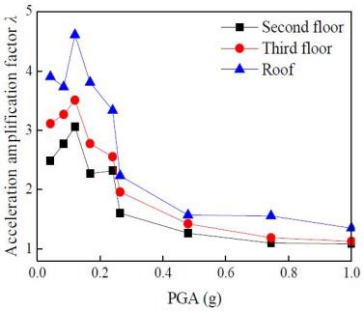

(c) Lanzhou wave

Fig. 10 Acceleration response of test specimen

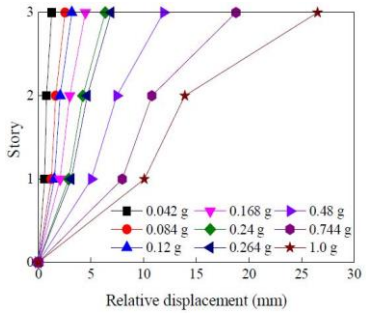

(a) El Centro wave

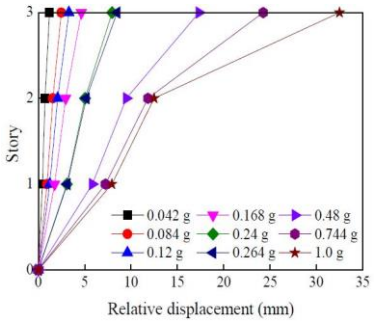

(b) Taft wave

Fig. 11 Maximum story displacement under each seismic load

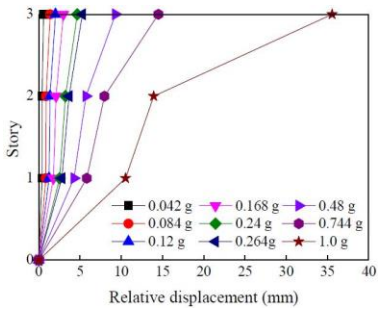

(c) Lanzhou wave

Fig. 11 Continued

Table 8 Maximum interstory drifts of the test specimen

PGA (g)	0.042	0.084	0.12	0.168	0.24	0.264	0.48	0.744	1.0
Maximum interstory drifts	1/3011	1/1452	1/1179	1/872	1/585	1/542	1/228	1/129	1/71

Table 9 Maximum link rotations of the test specimen

PGAs (g)	0.042	0.084	0.12	0.168	0.24	0.264	0.48	0.744	1.0
Link rotations/rad	0.003	0.006	0.007	0.009	0.014	0.015	0.035	0.063	0.114

displacement of each story increased when accelerations reached 0.48 g, 0.744 g, and 1.0 g. The increment of displacement of the third story was greater than that of the other stories because of the weld fracture at the link-to-braces joints. Table 8 and Table 9 provide the maximum interstory drifts and link rotations of the specimen under each seismic load, respectively. The maximum interstory drifts were 0.07%, 0.18%, and 0.44% when the PGA reached the corresponding values for "immediate occupancy," "life safety," and "collapse prevention" in Table 5, respectively; these interstory values of the specimen were less than the limitation for the EBF (as seen in Table 5).

3.5 Dynamic strain response

Dynamic strain response measurements from the strain gauges for the links, braces, beams, and columns indicate that the peak dynamic strain values increased with incremental increases in seismic load. Figs. 12, 13, and 14 show the dynamic strain curves at each point of interest during the El Centro, Taft, and Lanzhou waves with different PGAs, respectively. The ratio, $\varepsilon/\varepsilon_y$, characterizes the relative strain, where ε and ε_y are peak strain value and yield strain, respectively. When the PGA is less than 0.48 g, the strain at each point is lower than the yield value, and the specimen is in an elastic state. The strains in the link web were higher than strains in the link flange, which indicated that the links exhibited shear deformation. Strains in the link web were larger than the yield strain, while strains in the braces, beams, and columns remained lower than the yield strain for PGAs of 0.48 g, 0.744 g, and 1.0 g. These observations suggest that Y-HSS-EBF links enter a plastic stage to dissipate the energy, while the other structural

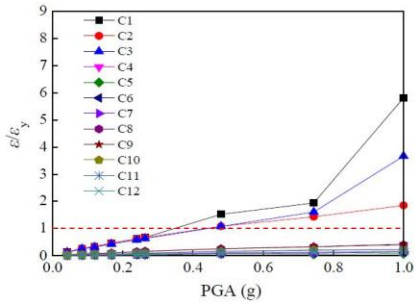

(a) Points in the first story

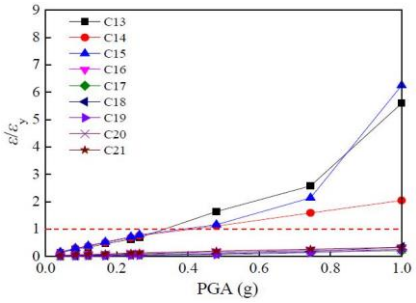

(b) Points in the second story

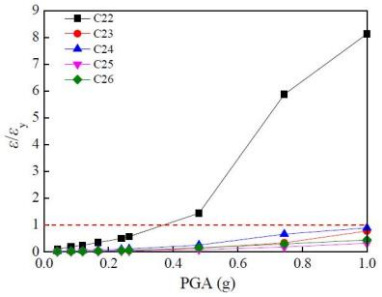

(c) Points in the third story

Fig. 12 Strain response during El Centro wave

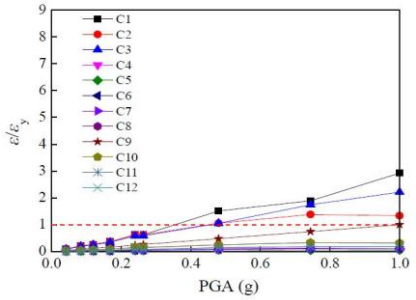

(a) Points in the first story

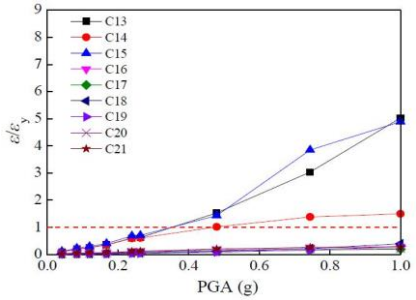

(b) Points in the second story

Fig. 13 Strain response during Taft wave

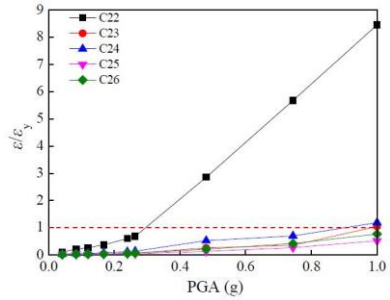

(c) Points in the third story

Fig. 13 Continued

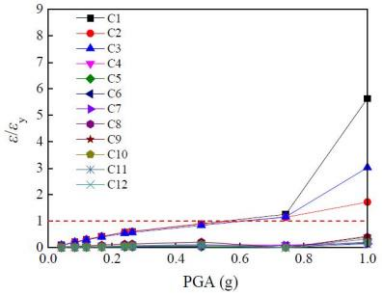

(a) Points in the first story

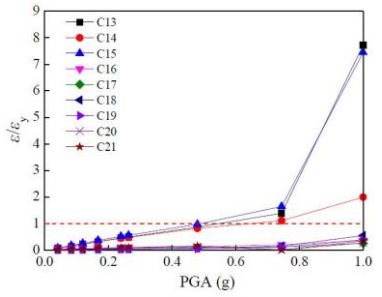

(b) Points in the second story

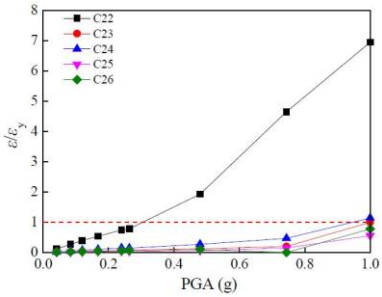

(c) Points in the third story

Fig. 14 Strain response during Lanzhou wave

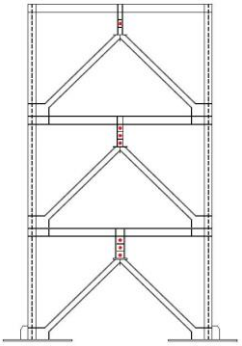

Fig. 15 Yielding locations

members remain in an elastic stage during an earthquake. According to the test results, the yielding locations appeared at link web in the specimen, as shown in Fig. 15.

4. Numerical simulation of experimental results

4.1 Finite element model of test specimen

The FEM of the test specimen was constructed using SAP2000. In the FEM, beam elements were used for the links, beams, columns, and braces, while shell elements were used for the slabs. Fig. 16 shows the FEM of the specimen in SAP2000. The boundary conditions were similar to the actual boundary conditions of the test specimen. All the DOFs of the column base bottom were constrained to consider the rigid connection between the column base and the shake table. The mechanical properties of steel given in Table 2 were used in the FEM. Nonlinear hinges were defined at the links, beams, columns, and braces. For shear link, the model presented in Tables 5-6 of FEMA-356 was considered for the nonlinear behavior (Fig. 17). The ultimate shear force of the shear link V_u=1.4V_p according to experimental results of shear links (Okazakia and Engelhardtb 2007). Moreover, the immediate occupancy deformation Δ_{IO}, life safety plastic deformation Δ_{LS} and collapse prevention deformation Δ_{CP} of the shear link were conducted using the parameters as suggested by Tables 5-6 of FEMA-356. To simulate the elastic and plastic seismic responses for the three-story Y-HSS-EBF specimen, and to compare the numerical analysis results with the test results, PGAs of 0.042 g, 0.084 g, 0.168 g, 0.264 g, 0.48 g, and 0.744 g were considered, along with ground motions of the El Centro, Taft, and Lanzhou waves for the specimen.

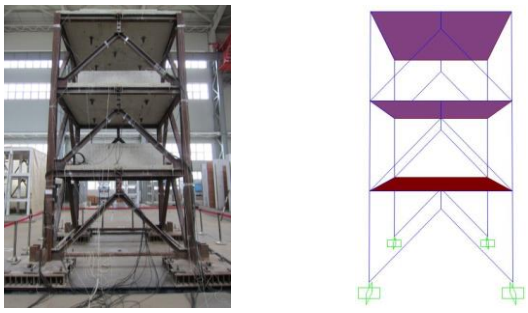

(a) Test specimen (b) FEM

Fig. 16 FEM of specimen in SAP2000

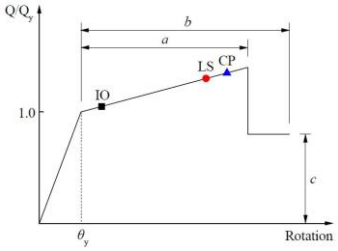

Fig. 17 Generalized force-deformation relation for shear link (FEMA-356)

Table 10 Comparisons of analysis and test maximum acceleration responses under different PGAs

Ground motion	PGA/g	Second floor			Third floor			Roof		
		a_A (g)	a_T (g)	a_A / a_T	a_A (g)	a_T (g)	a_A / a_T	a_A (g)	a_T (g)	a_A / a_T
El Centro wave	0.042	0.078	0.082	0.95	0.101	0.107	0.94	0.131	0.134	0.98
	0.084	0.161	0.173	0.93	0.233	0.218	1.07	0.302	0.277	1.09
	0.168	0.256	0.281	0.91	0.348	0.359	0.97	0.501	0.509	0.98
	0.264	0.423	0.405	1.04	0.523	0.509	1.03	0.87	0.767	1.13
	0.48	0.652	0.681	0.96	0.958	0.987	0.97	1.102	1.354	0.81
	0.744	0.958	0.915	1.05	1.050	1.222	0.86	1.513	1.883	0.80
Taft wave	0.042	0.068	0.065	1.05	0.076	0.084	0.90	0.128	0.139	0.92
	0.084	0.171	0.149	1.15	0.203	0.188	1.08	0.334	0.301	1.11
	0.168	0.257	0.289	0.89	0.356	0.370	0.96	0.473	0.529	0.89
	0.264	0.472	0.450	1.05	0.659	0.630	1.05	0.895	0.871	1.03
	0.48	1.009	0.860	1.17	1.251	1.085	1.15	1.342	1.565	0.86
	0.744	1.241	1.153	1.08	1.370	1.499	0.91	1.738	2.201	0.79
Lanzhou wave	0.042	0.109	0.098	1.11	0.128	0.123	1.04	0.166	0.154	1.08
	0.084	0.272	0.258	1.05	0.329	0.304	1.08	0.384	0.347	1.11
	0.168	0.212	0.231	0.92	0.516	0.566	0.91	0.417	0.388	1.07
	0.264	0.732	0.652	1.12	0.926	0.796	1.16	1.056	0.908	1.16
	0.48	0.717	0.798	0.90	1.038	0.898	1.16	1.131	0.989	1.14
	0.744	0.861	1.042	0.83	1.090	1.134	0.96	1.239	1.475	0.84

Note: a_A and a_T are the analysis and test value of the maximum acceleration, respectively

Table 11 Comparisons of analysis and test maximum relative displacements under different PGAs

Ground motion	PGA/g	Second floor			Third floor			Roof		
		Δ_A (g)	Δ_T (g)	Δ_A / Δ_T	Δ_A (g)	Δ_T (g)	Δ_A / Δ_T	Δ_A (g)	Δ_T (g)	Δ_A / Δ_T
El Centro wave	0.042	0.55	0.6	0.92	0.83	0.78	1.06	1.16	1.28	0.91
	0.084	1.17	1.24	0.94	1.78	1.66	1.07	2.67	2.54	1.05
	0.168	1.88	2.07	0.91	2.93	2.98	0.98	3.97	4.48	0.89
	0.264	2.97	3.13	0.95	5.01	4.65	1.08	7.23	6.91	1.05
	0.48	4.53	5.04	0.90	8.67	7.46	1.16	11.03	11.9	0.93
	0.744	6.68	7.97	0.84	12.12	10.79	1.12	15.26	18.77	0.81
Taft wave	0.042	0.4	0.43	0.93	0.74	0.71	1.04	1.09	1.2	0.91
	0.084	1.03	0.93	1.11	1.71	1.57	1.09	2.61	2.47	1.06
	0.168	1.53	1.76	0.87	2.65	2.93	0.90	4.23	4.64	0.91
	0.264	3.38	3.12	1.08	5.68	5.16	1.10	8.39	8.48	0.99
	0.48	6.22	5.82	1.07	11.45	9.49	1.21	15.32	17.34	0.88
	0.744	6.43	7.25	0.89	10.01	11.82	0.85	19.24	24.27	0.79
Lanzhou wave	0.042	0.37	0.38	0.97	0.44	0.39	1.13	0.62	0.58	1.07
	0.084	0.78	0.86	0.91	1.02	0.89	1.15	1.48	1.37	1.08
	0.168	1.58	1.77	0.89	2.24	2.09	1.07	3.13	2.98	1.05
	0.264	2.63	2.79	0.94	3.58	3.66	0.98	5.08	5.29	0.96
	0.48	3.82	4.27	0.89	5.28	5.72	0.92	7.92	9.3	0.85
	0.744	4.78	5.82	0.82	8.26	7.95	1.04	11.45	14.5	0.79

Note: Δ_A and Δ_T are the analysis and test value of the maximum relative displacement, respectively

4.2 Comparison of FEM analysis with test results

The natural frequency of the simplified analysis model was 5.79 Hz, which is 6% higher than that of the test

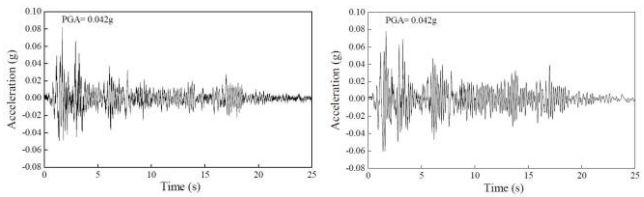

Experiment Analysis

(a) PGA=0.042 g

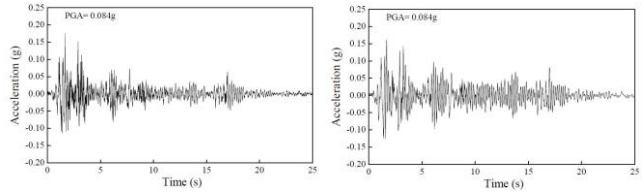

Experiment Analysis

(b) PGA=0.084 g

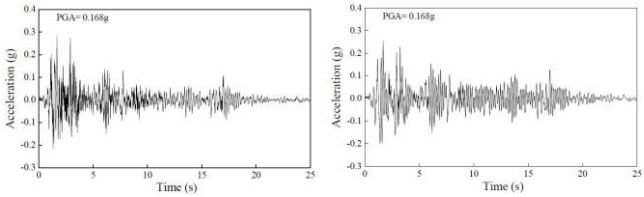

Experiment Analysis

(c) PGA=0.168 g

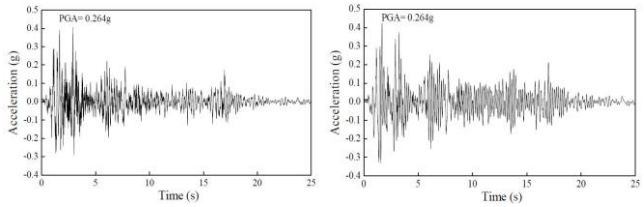

Experiment Analysis

(d) PGA=0.264 g

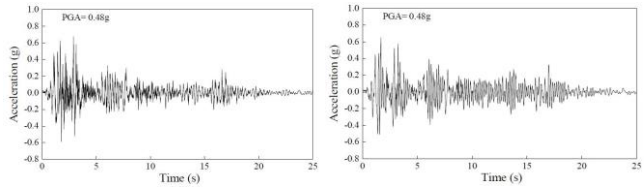

Experiment Analysis

(e) PGA=0.48 g

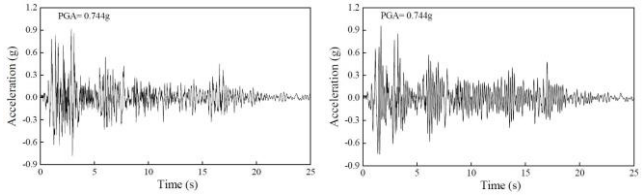

Experiment Analysis

(f) PGA=0.744 g

Fig. 18 Acceleration response time histories of experimental and analysis results

specimen. Tables 10 and 11 compare maximum acceleration responses and maximum story displacements from the numerical analysis and shake table test specimen during the various ground motions, respectively. Fig. 18 shows the

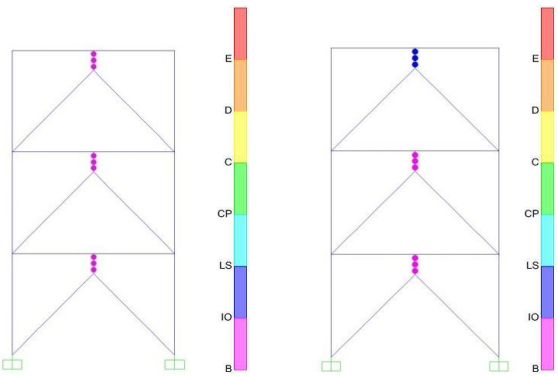

(a) PGA=0.48 g (b) PGA=0.744 g

Fig. 19 Plastic hinge distributions (El Centro wave)

acceleration response time histories in the second floor for the numerical analysis and the test specimen by using different PGAs of the El Centro wave.

The comparison between the simplified analysis and test specimen results indicate an error percentage of less than 10% under most loading cases. The error percentage for acceleration and displacement responses was more than 20% when the PGA reached 0.744 g; the weld fracture at the link-to-beam joints in the third floor of the test specimen could not be replicated in the numerical analysis. The acceleration response time histories were similar for the simplified analysis and the test specimen results. Fig. 19 shows the plastic hinge distributions of the FEM during the El Centro wave with PGAs of 0.48 g and 0.744 g, respectively. Compared to the strain responses in the specimen during the ground motions, the plastic hinge distributions in the FEM were similar to the test results. Thus, the numerical analysis using SAP2000 was observed to effectively simulate elastic and plastic seismic responses for Y-HSS-EBF structures during ground motions.

5. Advantages of HSS-EBFs compared to EBFs

Under the same design conditions, HSS-EBFs effectively reduce the overall steel weight because the HSS-EBFs require smaller member sections (relative to EBFs), considering the properties of HSS. In addition, HSS-EBFs offer seismic performance equivalent to that of EBFs, along with improved economy through reduced material costs (Lian and Su 2015). Moreover, the ratios of residual stress at critical points in the cross-section to yield stress are less for HSS columns than for conventional steel columns; the ratio of residual stress to yield stress (rather than the magnitude of residual stress itself) governs the reduction in strength. Hence, columns fabricated from HSS have a higher strength than that of columns of the same length and cross-section fabricated from conventional steel, when compared on a nondimensional basis (Rasmussen and Hancock 1992, 1995). The ratio is less for HSS because the magnitude of residual stress is largely independent of yield stress. Columns produced from HSS can have a higher slenderness reduction factor than the value adopted for columns manufactured from ordinary steel (Ban *et al.*

2011), thereby intrinsically reducing the influence of residual stress on the strength of HSS columns. It is stated that if the steel stress range not exceed the guidance that $1.5f_y$ for normal stresses or $1.5\ f_y/\sqrt{3}$ for shear stresses, for low cycle fatigue, the fatigue-resistant performance of HSS tubular structure is slightly higher than that of conventional steel structure (Vander *et al.* 1990). Using HSS for columns and beams can reduces the member sections and overall structure weight, which can reduce the damage to structures from earthquakes (Pocock 2006). Additionally, compared to EBFs, HSS-EBFs can provide more net area in the building because of the smaller cross-section of structure members.

6. Conclusions

In this study, the seismic response of a one-bay, three-story Y-HSS-EBF specimen was investigated using a shake table test, including the dynamic properties and acceleration, displacement, and strain responses. An FEM of the test specimen was conducted using SAP2000 software for the numerical simulation. Furthermore, a comparison between the experimental and numerical results was performed. The following conclusions can be drawn within the limitations of the research:

- The test specimen exhibited enough overall structural stiffness and sufficient safety; only localized damage occurred at a link in the specimen when the high seismic intensity earthquake was loaded. The Y-HSS-EBF is a safe dual system with reliable seismic performance.
- The test specimen stiffness decreased by 37.6% when a weld fracture occurred at a link, but there was no danger of collapse during the high seismic intensity earthquake.
- The maximum elastic and elastoplastic interstory drift in the test specimen for different PGAs were 1/872 and 1/71, respectively.
- During the high seismic intensity earthquake, the links entered a plastic stage to dissipate earthquake energy, while the structural members fabricated from HSS remained in an elastic stage.
- A useful agreement between the numerical analysis and experimental results was observed for the elastic and plastic seismic responses of the Y-HSS-EBF during ground motions. The FEM in SAP2000 provided an accurate prediction of the Y-HSS-EBF structure's behavior during the seismic loadings.

Acknowledgments

The authors are grateful for the partial financial support received from the National Natural Science Foundation of China (Grant No. 51178382 and 51478380).

References

Ban, H., Shi, G., Liu, Z., Shi, Y., Wang, Y., Xing, H. and Li, M. (2011), "Experimental study on overall buckling behavior of Q420 high strength equal angle members under axial compression", *J. Build. Struct.*, **32**(2), 60-67.

Berman, J.W. and Bruneau, M. (2007), "Experimental and analytical investigation of tubular links for eccentrically braced frames", *Eng. Struct.*, **29**(8), 1929-1938.

Bosco, M. and Rossi, P.P. (2009), "Seismic behaviour of eccentrically braced frames", *Eng. Struct.*, **31**(3), 664-674.

Bosco, M. and Rossi, P.P. (2013), "A design procedure for dual eccentrically braced systems: analytical formulation", *J. Constr. Steel Res.*, **80**(1), 440-452.

Chen, A.H., Xu, J.Q., Ran, L.I. and Li, H.L. (2012), "Corrosion resistance of high performance weathering steel for bridge building applications", *J. Iron Steel Res.*, **19**(6), 59-63.

Dubina, D., Stratan, A. and Dinu, F. (2008), "Dual high-strength steel eccentrically braced frames with removable links", *Earthq. Eng. Struct. Dyn.*, **37**(7), 1703-1720.

Dusicka, P., Itani, A. and Buckle, I. (2010), "Cyclic behavior of shear links of various grades of plate steel", *J. Struct. Eng.*, **136**(4), 370-378.

FEMA 356 (2000), Prestandard and commentary for the seismic rehabilitation of buildings, Washington, DC.

GB50011-2010 (2010), Code for seismic design of buildings, Beijing.

JGJ 99-98 (1998), Technical specification for steel structure of tall buildings, Beijing.

Li, Z.X. (2014), "Theory and technique of engineering structure experiments", Tianjin.

Lian, M., and Su, M.Z. (2015), "Seismic performance of eccentrically braced frames with high strength steel combination", *Steel Compos. Struct.*, **18**(6), 1517-1539.

Lin, K.C., Lin, C.C.J., Chen, J.Y. and Chang, H.Y. (2010), "Seismic reliability of steel framed buildings", *Struct. Safe.*, **32**(3), 174-182.

Longo, A., Montuori, R., Nastri, E. and Piluso, V. (2014), "On the use of hss in seismic-resistant structures", *J. Constr. Steel Res.*, **103**, 1-12.

Mansour, N., Christopoulos, C. and Tremblay, R. (2011), "Experimental validation of replaceable shear links for eccentrically braced steel frames", *J. Struct. Eng.*, **137**(10), 1141-1152.

Montuori, R., Nastri, E. and Piluso, V. (2014), "Rigid-plastic analysis and moment-shear interaction for hierarchy criteria of inverted Y EB-Frames", *J. Constr. Steel Res.*, **95**(4), 71-80.

Montuori, R., Nastri, E. and Piluso, V. (2014), "Theory of plastic mechanism control for eccentrically braced frames with inverted y-scheme", *J. Constr. Steel Res.*, **92**, 122-135.

Okazaki, T. and Engelhardt, M.D. (2007), "Cyclic loading behavior of EBF links constructed of ASTM A992 steel", *J. Constr. Steel Res.*, **63**(6), 751-765.

Pocock, G. (2006), "High strength steel use in Australia, Japan and the US", *Struct. Engineer*, **84**(21), 27-30.

Rasmussen, K.J.R. and Hancock, G.J. (1992), "Plate slenderness limits for high strength steel sections", *J. Constr. Steel Res.*, **23**(1), 73-96.

Rasmussen, K.J.R. and Hancock, G.J. (1995), "Tests of high strength steel columns", *J. Constr. Steel Res.*, **34**(1), 27-52.

Shayanfar, M.A., Barkhordari, M.A. and Rezaeian, A.R. (2012), "Experimental study of cyclic behavior of composite vertical shear link in eccentrically braced frames", *Steel Compos. Struct.*, **12**(1), 13-29.

Shim, C.S., Whang, J.W., Chung, C.H. and Lee, P.G. (2011), "Design of double composite bridges using high strength steel", *Procedia Eng.*, **14**(7), 1825-1829.

Tokgoz, S., Dundar, C. and Tanrikulu, A.K. (2012), "Experimental behaviour of steel fiber high strength reinforced concrete and composite columns", *J. Constr. Steel Res.*, **74**(7), 98-107.

Vander, V. G. J., De, B. J. and Wardenier, J. (1990), "Low cycle fatigue of tubular T- and X-joints", *Proceedings of 3rd*

international symposium on tubular structures, Lappeenranta, Finland.
Wang, Y.B., Li, G.Q., Cui, W. and Chen, S.W. (2014), "Seismic behavior of high strength steel welded beam-column members", *J. Constr. Steel Res.*, **102**(11), 245-255.

CC